Solid organic-coated ammonium sulfate particles at high relative humidity in the summertime Arctic atmosphere

Rachel M. Kirpes[a], Ziying Lei[b,1], Matthew Fraund[c,2], Matthew J. Gunsch[a], Nathaniel W. May[a,3], Tate E. Barrett[d], Claire E. Moffett[e], Andrew J. Schauer[f], Becky Alexander[g], Lucia M. Upchurch[h,i], Swarup China[j], Patricia K. Quinn[i], Ryan C. Moffet[c,4], Alexander Laskin[j,5], Rebecca J. Sheesley[d,e], Kerri A. Pratt[a,k,6], and Andrew P. Ault[a,6]

[a]Department of Chemistry, University of Michigan, Ann Arbor, MI 48109; [b]Department of Environmental Health Sciences, University of Michigan, Ann Arbor, MI 48109; [c]Department of Chemistry, University of the Pacific, Stockton, CA 95211; [d]Institute of Ecological, Earth, and Environmental Sciences, Baylor University, Waco, TX 76798; [e]Department of Environmental Science, Baylor University, Waco, TX 76798; [f]Department of Earth and Space Sciences, University of Washington, Seattle, WA 98195; [g]Department of Atmospheric Sciences, University of Washington, Seattle, WA 98195; [h]Joint Institute for the Study of the Atmosphere and Ocean, University of Washington, Seattle, WA 98115; [i]Pacific Marine Environmental Laboratory, National Oceanic and Atmospheric Administration, Seattle, WA 98115; [j]Environmental Molecular Sciences Laboratory, Pacific Northwest National Laboratory, Richland, WA 99352; and [k]Department of Earth and Environmental Sciences, University of Michigan, Ann Arbor, MI 48109

Edited by Mark Thiemens, University of California San Diego, La Jolla, CA; received March 12, 2021; accepted January 25, 2022

The ability of atmospheric aerosols to impact climate through water uptake and cloud formation is fundamentally determined by the size, composition, and phase (liquid, semisolid, or solid) of individual particles. Particle phase is dependent on atmospheric conditions (relative humidity and temperature) and chemical composition and, importantly, solid particles can inhibit the uptake of water and other trace gases, even under humid conditions. Particles composed primarily of ammonium sulfate are presumed to be liquid at the relative humidities (67 to 98%) and temperatures (−2 to 4 °C) of the summertime Arctic. Under these atmospheric conditions, we report the observation of solid organic-coated ammonium sulfate particles representing 30% of particles, by number, in a key size range (<0.2 μm) for cloud activation within marine air masses from the Arctic Ocean at Utqiaġvik, AK. The composition and size of the observed particles are consistent with recent Arctic modeling and observational results showing new particle formation and growth from dimethylsulfide oxidation to form sulfuric acid, reaction with ammonia, and condensation of marine biogenic sulfate and highly oxygenated organic molecules. Aqueous sulfate particles typically undergo efflorescence and solidify at relative humidities of less than 34%. Therefore, the observed solid phase is hypothesized to occur from contact efflorescence during collision of a newly formed Aitken mode sulfate particle with an organic-coated ammonium sulfate particle. With declining sea ice in the warming Arctic, this particle source is expected to increase with increasing open water and marine biogenic emissions.

Arctic aerosol | atmospheric chemistry | aerosol phase | secondary aerosol | marine biogenic aerosol

In the atmosphere, aerosols impact climate by directly scattering or absorbing solar radiation and by taking up water to act as cloud condensation nuclei (CCN) or ice nucleating particles (INPs), thereby modifying cloud properties. Water uptake is governed by individual particle physicochemical properties, including composition, phase, size, and morphology (1, 2). Particle phase impacts particle reactivity (3), water uptake (4), gas partitioning (3), optical properties (5), and CCN and INP efficiencies (1). Particles with high viscosity impact heterogeneous reactions by inhibiting diffusion of gaseous species into particles (6, 7). Thus, it is critical to understand the phase behavior of a particle to be able to predict aerosol impacts on climate. Water uptake calculations are typically driven by thermodynamic predictions incorporated into global climate models (8). However, laboratory and field evidence (9, 10), as well as modeling predictions (8), have shown that organic particles are more often in a solid or viscous state than previously assumed.

Despite the evidence for abundant solid or glassy organic particles (11, 12), ubiquitous hygroscopic inorganic components, such as ammonium sulfate, are presumed to be primarily present as ions dissolved in aqueous particles in the marine boundary layer due to the high relative humidity (RH) (13, 14). When considering the phase of ammonium sulfate at 293 K, there is a well-known hysteresis effect where a solid ammonium sulfate particle undergoes a phase transition to an aqueous

Significance

Physical and chemical properties of individual atmospheric particles determine their climate impacts. Hygroscopic inorganic salt particles mixed with trace amounts of organic material are predicted to be liquid under typical tropospheric conditions in the summertime Arctic. Yet, we unexpectedly observed a significant concentration of solid particles composed of ammonium sulfate with an organic coating under conditions of high relative humidity and low temperature. These particle properties are consistent with marine biogenic-derived new particle formation and growth, with particle collision hypothesized to result in the solid phase. This particle source is predicted to have increasing relevance in the context of declining Arctic sea ice and increasing open water, with impacts on clouds, and therefore climate.

Author contributions: K.A.P. and A.P.A. designed research; R.K., Z.L., M.F., M.J.G., N.W.M., T.E.B., C.E.M., A.J.S., and L.M.U. performed research; S.C., P.K.Q., R.C.M., A.L., and R.J.S. contributed new reagents/analytic tools; R.K., Z.L., M.F., M.J.G., N.W.M., T.E.B., C.E.M., A.J.S., B.A., L.M.U., K.A.P., and A.P.A. analyzed data; and R.K., K.A.P., and A.P.A. wrote the paper.

The authors declare no competing interest.

This article is a PNAS Direct Submission.

[1]Present address: Department of Atmospheric Sciences, Texas A&M University, College Station, TX, 77843.

[2]Present address: Chemical Sciences Division, Lawrence Berkeley National Laboratory, Berkeley, CA 94720.

[3]Present address: Physical Sciences Division, University of Washington Bothell, Bothell, WA 98011.

[4]Present address: Sonoma Technology, Petaluma, CA 94954.

[5]Present address: Department of Chemistry, Purdue University, West Lafayette, IN 47907.

[6]To whom correspondence may be addressed. Email: aulta@umich.edu or prattka@umich.edu.

This article contains supporting information online at http://www.pnas.org/lookup/suppl/doi:10.1073/pnas.2104496119/-/DCSupplemental.

Published March 28, 2022.

particle at 78% RH when RH is increasing, while a liquid particle will not crystallize when drying until 34% RH (15). Thus, since one of the most common mechanisms for sulfate [$SO_4^{2-}{}_{(aq)}$] formation is aqueous phase oxidation of SO_2, and the RH over the Arctic Ocean does not go below 34% (16), it is commonly assumed that ammonium sulfate is present as dissolved ions in aqueous particles in the summertime Arctic. Even at temperatures near 0 °C, the phase transition to a solid is not predicted for pure ammonium sulfate at typical ambient RH values (~60 to 100%) by the ammonium sulfate phase diagram (15).

In this study we report the surprising observation of solid ammonium sulfate particles with organic coatings in the accumulation mode collected in marine air masses in the summertime Arctic at low temperatures (−2 to +4 °C) and high RH (67 to 98%), for which ammonium sulfate is predicted to be present in aqueous particles. These particles were characterized using a multimodal microspectroscopic approach to determine their chemical composition, phase, and morphology. A combination of laboratory studies, thermodynamic modeling, and attribution of sources and formation processes is used to explain these unexpected results and their potential implications for atmospheric chemistry in cold, humid environments, including the summertime Arctic marine boundary layer.

Results and Discussion

Solid Particles Observed at Low Temperature and High RH. Ambient particles were collected at the coastal Arctic location of Utqiaġvik, AK during August to September 2015, at ambient temperatures from –2 to +4 °C and RHs between 67 and 98% within marine air masses. Microscopic analysis revealed a unique type of particle that was predominantly ammonium sulfate, the phase of which was unexpectedly solid with a complex morphology (Fig. 1). The physical properties of these particles were investigated using atomic force microscopy (AFM), which demonstrated the tall nature of the particles, with heights of 150 to 200 nm measured for 130- to 500-nm projected area diameter (d_{pa}) particles (Fig. 1 *A* and *B*). Upon impaction, these particles spread a similar amount as solid particles and far less than aqueous particles (17, 18), indicating these ambient particles existed in a solid or viscous phase. AFM phase images revealed particles with complex structure, showing a difference in particle phase (19) between the main particle and distinct smaller particle(s) on its surface (Fig. 1*C*). Scanning electron microscopy (SEM) imaging in transmission mode showed that most of these round particles contained small (~20 nm) cubic sulfate particles on the surface (Fig. 1*D*), distinct from the ammonium sulfate in the core (20). SEM images collected at a 75° tilt in back-scattering mode further demonstrated the tall, hemispherical nature of these particles (Fig. 1*F*), in comparison to other flat, liquid ambient particle types observed within the same samples (*SI Appendix*, Fig. S1). This tilt method has previously been used to show solid organic particles formed in agricultural areas (10). To our knowledge, this tall morphology has not been previously observed for ambient particles in the Arctic or beyond, suggesting it is unique to the particle composition, observed atmospheric conditions, and particle's history since its formation.

The physical properties of these ambient particles were compared to the morphology of laboratory-generated solid (RH = 15%, effloresced) ammonium sulfate particles, as well as liquid (RH = 50%, deliquesced) inorganic sulfate particles from Olson et al. (18) (Fig. 2). Particle phase can be inferred by the extent of spreading, determined by the particle radius and height following inertial impaction onto a substrate at ambient pressure. AFM height traces (25 to 72 particles per trace) showed that the tall ambient particles were comparable to

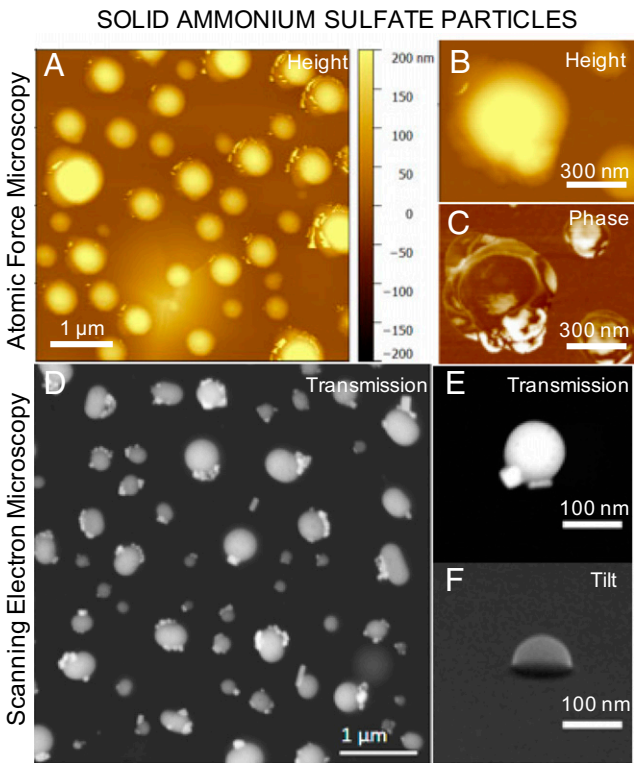

Fig. 1. AFM (*A* and *B*) height and (*C*) phase images demonstrating the unique morphology of the observed ammonium sulfate particles (15 September 2015 00:00 to 08:00 sample). SEM (*D*) transmission electron detector image (16 September 2015 00:00 to 08:00 sample), (*E*) transmission electron detector image (5 to 6 September 2015 16:00 to 00:00 sample) and (*F*) secondary electron detector 75° tilted image (7 September 2015 00:00 to 08:00 sample) further demonstrating the morphology of these particles. All sample times are given in Alaska Daylight Time.

similar diameter solid laboratory-generated ammonium sulfate particles, while the aqueous laboratory-generated sulfate particles were much shorter (Fig. 2*A*). Spreading ratios are similar for the ambient (2.0 ± 0.1) and solid laboratory (1.43 ± 0.08)

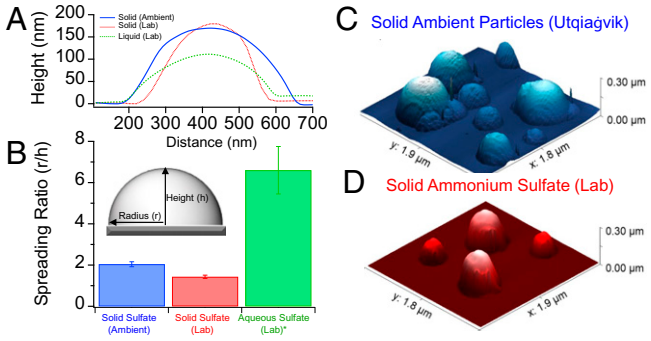

Fig. 2. (*A*) Average AFM height traces for ambient ammonium sulfate-dominant particles (16 September 2015 00:00 to 08:00 Alaska Daylight Time sample) (blue), as well as solid (red) and liquid (green) ammonium sulfate particles generated in the laboratory. Liquid ammonium sulfate plus sulfuric acid particles (green) are from Olson et al. (18). (*B*) spreading ratios (radius/height) from AFM for ambient, solid (laboratory), and liquid (laboratory) (70, 72, and 25 particles measured, respectively) following method in Olson et al. (18) with error bars at 95% confidence interval. The inset cartoon shows how radius and height are defined for calculating the spreading ratio. AFM three-dimensional height profiles for (*C*) ambient ammonium sulfate-dominant particles from Utqiaġvik and (*D*) solid laboratory-generated ammonium sulfate particles.

particles and far less than for the aqueous laboratory particles (7 ± 1) (Fig. 2*B*). Three-dimensional AFM height images further demonstrated the similar morphology of the tall ambient (Fig. 2*C*) and solid laboratory-generated ammonium sulfate particles (Fig. 2*D*), indicating the ambient particles exhibited a solid phase (21). To examine whether the ambient particles were capable of deliquescing and spreading substantially on the substrate, RH cycling experiments were conducted for the ambient particles where RH was increased up to 85%, above the deliquescence RH of ammonium sulfate, and then decreased to 30%. Low spreading ratios were still observed after cycling, confirming the particles did not deliquesce to fully liquid particles on the substrate and spread (see details in *SI Appendix* and *SI Appendix*, Fig. S1).

Chemical Composition and Phase Separation. The chemical composition of the individual particles was determined to investigate its role in the observed morphology and phase. SEM coupled with energy dispersive X-ray spectroscopy (SEM-EDX) identified carbon, oxygen, and sulfur in the individual particles (Fig. 3*A* and Fig. S3), indicative of sulfate and organics. Notably, these particles were extremely sensitive to the electron beam, characteristic of ammonium sulfate (22). Other elements associated with sea spray (e.g., Na, Mg, K, Ca, and Cl) were not observed in these particles. Scanning transmission X-ray microscopy with near-edge X-ray absorption fine structure (STXM-NEXAFS) spectra of individual particles over the sulfur L-edge confirmed the presence of inorganic sulfate [S(VI)] in the particles (Fig. S4) (23). AFM coupled with photothermal infrared spectroscopy (AFM-PTIR) was used to identify functional groups present in particles smaller than the optical diffraction limit (17, 24). AFM-PTIR analysis of individual particles identified ammonium sulfate, with characteristic $\nu_{as}(SO_4^{2-})$ and $\delta(NH_4^+)$ modes at 1,098 cm^{-1} and 1,420 cm^{-1}, respectively (13, 17), a bisulfate $\nu_{as}(HSO_4^-)$ mode at 1,260 cm^{-1}, and a $\delta(H_2O)$ mode at 1,726 cm^{-1} (13) (Fig. 3*B* and additional PTIR spectra in Fig. S5). The location of an ammonium $\delta(NH_4^+)$ mode at 1,420 cm^{-1} is consistent with solid ammonium sulfate, based on prior efflorescence studies (13).

Trace organic compounds impact the phase (25) and physical properties [deliquescence, efflorescence, and crystallization (15, 26–28)] of ammonium sulfate particles. The presence of organics in the ambient particles was confirmed by STXM-NEXAFS mapping over the carbon K-edge, which showed organic components coating the primarily inorganic particles (Fig. 3*C*). Inclusions of sp^2 carbon were also observed on the organic/inorganic interface of a few particles (Fig. 3*C*), indicative of material not soluble in the organic phase and further demonstrating the complex multiphase nature of these particles. Though commonly associated with soot, sp^2 carbon has also been attributed to marine biogenic sources (29, 30). Organic coatings on ammonium sulfate particles were recently observed during summertime in the Norwegian Arctic, including some particles with soot inclusions in the organic coating, though these particles were liquid when collected based on extensive spreading (31). Organic volume fractions within the individual ambient particles in this study were determined based on the STXM-NEXAFS data. Two distinct components were defined: an organic coating (average 89% organic, 11% inorganic) and an inorganic core (average 3% organic, 97% inorganic) (Fig. 3 *D* and *E*). The thickness of the inorganic and organic components from the edge to center of each particle was determined based on the organic volume fraction, further demonstrating the presence of an organic dominant coating (100- to 150-nm thickness) and inorganic dominant core (Fig. 3 *D* and *E*). The solubility of organic compounds decreases with temperature (32); therefore, at the observed temperatures (–2° to +4 °C), the organic coatings likely formed via liquid–liquid phase

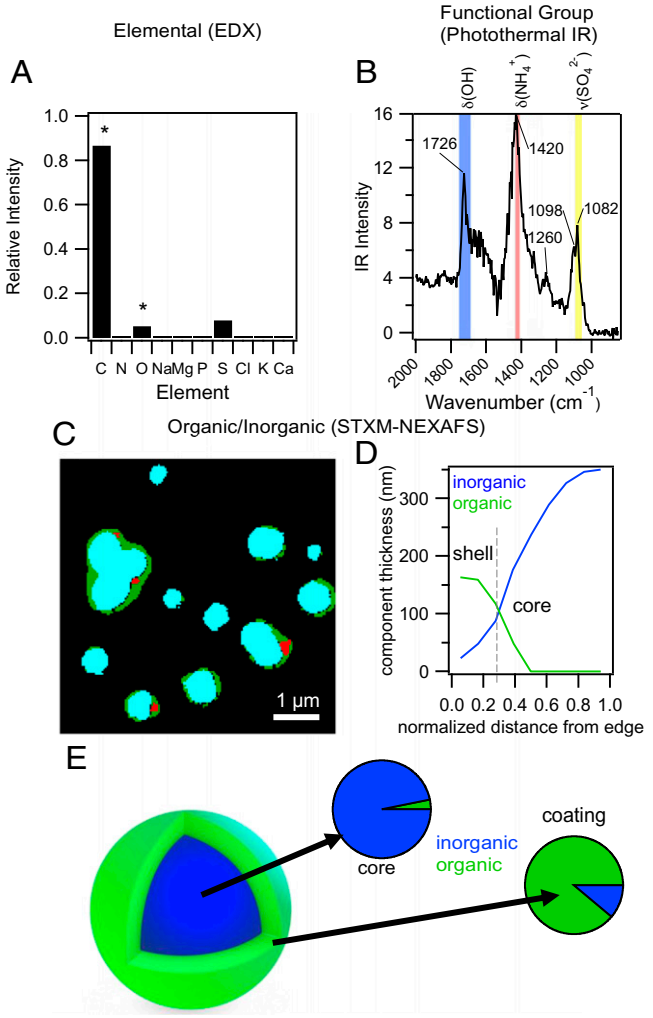

Fig. 3. (*A*) Average EDX elements present in the ambient ammonium sulfate particles from all samples (*C and O peaks contain some signal from substrate background) and (*B*) a representative AFM-PTIR spectrum of an individual ambient ammonium sulfate particle. (*C*) STXM-NEXAFS map showing the distribution of inorganic (blue), organic (green), and sp^2 carbon (red) within individual sulfur-rich particles. (*D*) Average organic and inorganic fractions for the coating and core regions of sulfur-rich particles determined by STXM-NEXAFS. (*E*) Distribution of inorganic and organic thickness from coating to core of a representative ambient organic-coated ammonium sulfate particle, determined by STXM-NEXAFS.

separations due to the lower surface energy of that structure (33). However, the sampled particles observed herein were solid, which means the ammonium sulfate core effloresced in the atmosphere prior to collection. This efflorescence likely concentrated the organic material at the surface, leading to the formation of a more viscous organic phase.

For each time period when the solid particles were collected, RH <81% was observed during a portion of the air mass trajectory (*SI Appendix*, *Discussion of Impaction and Analysis of Solid Particles* and Fig. S6). During Arctic Ocean air mass sampling, ambient RH ranged from 67 to 98%, with 38% of the sampling time at RH <81%. Aqueous ammonium sulfate is metastable (i.e., supersaturated) at RH <81% (13), the deliquescence RH of ammonium sulfate for the sampling temperatures (15, 34). In a metastable phase, it is thermodynamically favorable for particles to effloresce and form a solid phase, but without a surface to overcome the free energy barrier necessary to nucleate a new phase (35), the particles remain aqueous. Contact

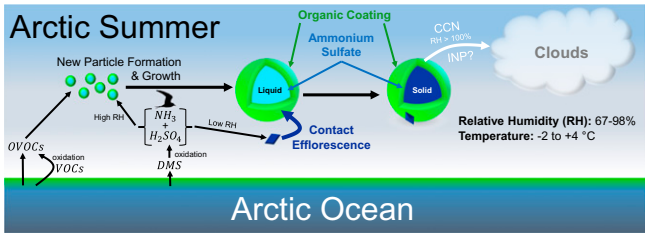

Fig. 4. Illustration of observed solid ammonium sulfate particles with organic coatings, and associated processes, during summer for Arctic Ocean air masses. The particles at cloud-nucleating sizes were surprisingly observed to be solid, rather than aqueous, despite sampling RHs >40%, which is the efflorescence RH of ammonium sulfate at the sampling temperatures. The particle composition and air mass influence are consistent with observational and modeling studies showing new particle formation via sulfuric acid (H_2SO_4, from DMS oxidation) and ammonia (NH_3), with condensational growth from sulfate and highly oxygenated organic molecules from oxidized volatile organic compounds (OVOCs) (39, 40, 42, 43). DMS, VOCs, and OVOCs are emitted from the Arctic Ocean (41), while ammonia (NH_3) is attributed to birds in the Arctic (42). Modeling suggests that this process increases CCN concentrations (42). CCN activation at supersaturated RH is likely (47), with these solid particles also potentially acting as INPs (48), thereby contributing to Arctic climate feedbacks. Aitken mode solid sulfate particles, formed and present at portions of the air mass trajectory with RH <81%, colliding with accumulation mode organic-coated ammonium sulfate particles are hypothesized to induce contact efflorescence, as observed in the laboratory (36).

efflorescence occurs when a solid particle collides with a metastable particle and provides a surface that facilitates efflorescence at an RH much higher than the efflorescence RH (34) [40% for ammonium sulfate at the sampling temperatures (15)]. Recently, it has been shown in laboratory experiments that solid ammonium sulfate particles induce efflorescence when they collide with phase-separated particles composed of an organic shell and aqueous ammonium sulfate core (36). Therefore, small, solid sulfate particles, formed at RH <81%, colliding with larger core-shell (ammonium sulfate-organic) particles at <81%, can explain the solid organic-coated ammonium sulfate particle structure with cubic sulfate protrusions at the surface observed by AFM and SEM (Fig. 1). Therefore, we hypothesize that contact efflorescence led to these unexpected solid sulfate particles.

Proposed Marine Biogenic Source and Formation Mechanism. The organic-coated ammonium sulfate particles were primarily observed under Arctic Ocean air mass influence from the Beaufort Sea (*SI Appendix*, Fig. S6), with minimal anthropogenic influence (37). Bulk aerosol composition, including sulfur isotope analysis, supports a marine biogenic aerosol source, as discussed in *SI Appendix*. During these marine air masses, the full aerosol size distribution has modes in both the Aitken and accumulation diameter ranges (*SI Appendix*, Fig. S2), which is representative and typical of the summertime Arctic (38). The number fraction of the observed solid organic-coated ammonium sulfate particles increased with decreasing particle diameter from 0.56 μm d_{pa} to 0.18 μm (31 ± 2%, by number) then slightly decreased to the lower size collection limit of 0.13 μm d_{pa} (23 ± 5%, by number) (*SI Appendix*, Fig. S2) (37). At less than 0.2 μm d_{pa}, ~30% of the total particles, by number, corresponded to these solid, organic-coated ammonium sulfate particles, associated with a peak in the size distribution at ~120 nm (*SI Appendix*, Fig. S2) (37), indicating that a significant fraction of the observed particle number concentration exhibited a solid phase in a key size range for CCN activation. The Aitken mode particles were below the lower size collection limit, which prohibited microscopic analysis; however, these particles (mode diameter ~25 nm) are notably similar in size to the sulfate edge protrusions on the larger solid particles, supporting the hypothesis of Aitken mode particles colliding with accumulation mode particles.

The typical summertime Arctic bimodal aerosol size distribution has been explained, through observations and modeling by Croft et al. (38), by new particle formation and growth resulting in Arctic Aitken mode particles (<0.1 μm) and further condensation leading to the accumulation mode (0.1 to 1.0 μm). Recently, Beck et al. (39) showed summertime observations at Svalbard of particle nucleation via sulfuric acid (from marine dimethylsulfide [DMS] oxidation) and ammonia, followed by condensation of sulfate, methanesulfonate, and highly oxygenated organic molecules, with growth to CCN sizes. Earlier measurements showed that ammonium sulfate is the main component of new particles during summertime at Svalbard (40) and that oxygenated volatile organic compounds are emitted from open water during summer in the Canadian Archipelago (41). Modeling has shown that ammonia emissions from sea birds react with sulfuric acid, from DMS oxidation, and contribute to new particle formation and increased cloud droplet number concentrations across the Arctic, including over the Beaufort Sea, an area where elevated ammonia concentrations were previously observed (42). Further Arctic air quality modeling by Ghahremaninezhad et al. (43) suggests that DMS oxidation and resulting new particle formation and growth leads to significant enhancements in sulfate particles up to 0.2 μm at high latitudes (>70°N), with strong enhancements up to 1 μm at lower latitudes (<70°N). Indeed, frequent aerosol growth events, with >0.1-μm particles consisting primarily of organics and sulfate, were observed simultaneously at the Canadian Archipelago Arctic sites of Eureka and Alert, located 480 km apart, during August to September 2015 (44). The observed bimodal aerosol size distribution (*SI Appendix*, Fig. S2) resulting from the regional new particle formation and growth events supports the hypothesized contact efflorescence occurring when a newly formed Aitken mode sulfate particle, formed at a portion of the air mass trajectory at <81% RH (*SI Appendix*, Fig. S6), collides with an accumulation mode organic-coated ammonium sulfate particle at RH <81%. Therefore, this new particle formation and growth mechanism, dominated by marine biogenic sulfate, is consistent with the particle properties measured in our study at Utqiaġvik, AK (71°N) with marine air mass influence from the Beaufort Sea (Fig. 4).

Conclusions

The observation of solid, organic-coated ammonium sulfate particles in the Arctic boundary layer has significant implications for regional atmospheric chemistry, cloud formation, and climate feedbacks. The solid phase of these particles is hypothesized to have formed through contact efflorescence when an Aitken mode solid sulfate particle collided with an accumulation mode organic-coated ammonium sulfate particle, with the ammonium sulfate core in a metastable (i.e., supersaturated) state, which has recently been observed in the laboratory (36). The unexpected solid phase and solid organic coating on these particles likely inhibited trace gas and water uptake at subsaturated RH (45, 46). Despite the increased timescale expected for water uptake, glassy organic particles with ammonium sulfate cores are expected to activate as CCN at elevated water supersaturation, based on room-temperature measurements (47). Notably, solid ammonium sulfate particles also have a higher refractive index than liquid particles and can serve as INPs via deposition freezing (48). These particles may be a previously unconsidered source of INPs in the Arctic, where mixed-phase clouds are important for the surface energy budget and yet challenging to simulate (49). Recent incorporation of inferred viscosity into a global model predicted secondary

organic aerosol to be mostly liquid or semisolid in the boundary layer, with glassy particles mostly existing in the upper troposphere (8). Yet, here we demonstrate the presence of organic-coated ammonium sulfate particles that were solid under summertime Arctic conditions with low temperature and high RH. This highlights the need to further investigate aerosol phase and water uptake at temperatures near freezing under humid conditions.

The observed organic-coated ammonium sulfate particles are consistent with new particle formation from the reaction of marine-derived sulfuric acid and ammonia, followed by condensation of biogenic sulfate and highly oxygenated organic molecules, with growth to cloud activation sizes (39). Atmospheric new particle formation and growth is simulated to be the dominant source of Aitken and accumulation mode particles and an important source of CCN to the Arctic atmosphere (38, 42), which is warming faster than elsewhere on Earth (50). Secondary marine aerosol has also been shown to be the dominant source of CCN in marine regions, including the Arctic (51). Given the prevalence of this formation mechanism across the Arctic (42), especially in areas of open water (39), the phase of the particles observed in this study is important to consider, especially in the rapidly warming Arctic with increasing open water (52) and thereby increasing marine biogenic emissions.

Methods

Sample Collection. Atmospheric particles were sampled near Utqiaġvik, AK using a three-stage microanalysis particle sampler for individual particle microscopy analyses (8-h samples), a TSP sampler for sulfur isotope analysis and ion chromatography analysis, and a PM_1 Berner-type multijet cascade impactor for submicron particle ion chromatography analysis; details of each sampling method are described below and in *SI Appendix*. Meteorological data, including RH and temperature, were obtained from the National Oceanic & Atmospheric Administration (NOAA) Barrow Observatory and the Department of Energy (DOE) Atmospheric Radiation Measurement (ARM) North Slope of Alaska Observatory.

Atmospheric particles for microscopy analysis were sampled at an Arctic coastal tundra field site (71°16′30″ N, 156°38′26″ W) from 21 August to 30 September 2015, as described by Gunsch et al. (37). Individual particles (70- to 400-nm aerodynamic diameter) were collected using a microanalysis particle sampler (MPS) (MPS-3; California Measurements Inc.) onto transmission electron microscopy (TEM) grid substrates (carbon Type-B Formvar film copper grids; Ted Pella Inc.). Samples were collected for ∼8 h then sealed in airtight containers and stored in the dark at room temperature prior to analysis. Here we focus on 22 samples (*SI Appendix*, Table S3) that contained significant number fractions (>15%) of the ammonium sulfate particle type identified previously by Gunsch et al. (37). Discussion of particle sampling and analysis of solid particles is included in *SI Appendix*.

Laboratory Particle Generation. Ammonium sulfate aerosol particles were generated for individual particle microscopy analysis using an atomizer from a 10 μM solution (99.7%; Fisher Scientific). Particles 200 nm in diameter were size-selected using a differential mobility analyzer (DMA) (model 3082; TSI Inc.) to be representative of the observed ambient particle size mode. The RH within the DMA was controlled using diffusion driers upstream to generate solid particles at 15% RH. Particles were impacted onto TEM grids for offline analysis using an MPS.

Single-Particle Microscopy Measurements. The individual particle MPS samples on TEM grid substrates were analyzed by computer-controlled SEM-EDX using an FEI Quanta scanning electron microscope with field emission gun operating at 20-keV accelerating voltage. The instrument is equipped with a high angle annular dark field detector and energy-dispersive X-ray detector (EDAX, Inc.) to provide information on the size, morphology, and elemental composition of individual particles. K-means clustering of the EDX data identified unique particle classes, as described by Gunsch et al. (37) and references therein. Additional SEM images were collected using a secondary electron detector with the sample tilted 75° to provide additional information on particle three-dimensional morphology (10).

AFM-PTIR was used to further probe the morphology and chemical composition of individual particles using a nanoIR2 (Anasys Instruments). AFM images were collected in contact mode at a 0.75-Hz scan rate over a 5-μm × 5-μm area on the copper grid bar of the TEM grid substrate in order to measure the diameter and height of individual particles, according to an established method for AFM-PTIR application to aerosol particles (17, 53). Spreading ratios and associated errors (95% confidence interval) were calculated following the method in Olson et al. (18). IR spectra were collected over the 900 to 3,600 cm^{-1} range at 4 cm^{-1} per point resolution. Additional AFM images were collected in tapping mode to provide information on particle phase (19).

STXM-NEXAFS was conducted at the Canadian Light Source Beamline 10ID-1. Analysis was conducted over the carbon K-absorption edge and sulfur L-absorption edge to distinguish carbon and sulfur oxidation states present in the individual particles, using a previously described method (23, 54). Briefly, X-ray energies are selected with a monochromator and raster-scanned across the sample. Images at closely spaced X-ray energies are combined to create an image stack, and X-ray spectra are converted to optical density using the Beer–Lambert law. Pre-edge/postedge ratios of X-ray absorption over the carbon K-absorption edge (280 to 320 eV) were used to create a map showing the relative contribution of organic and inorganic components in individual particles. Sulfur L-absorption edge spectra were collected over the 168- to 176-eV range. The ratio of peaks at 173.2 and 171.1 eV was used to assess the relative contribution of different sulfur oxidation states [S(V) and S(VI)].

Data Availability. All study data are included in the article and/or *SI Appendix*.

ACKNOWLEDGMENTS. This study was supported by the NOAA Climate Program Office of Atmospheric Chemistry, Carbon Cycle, and Climate Program (NA14OAR4310149), NSF CAREER Award (CHE-1654149), and DOE Early Career Award (DE-SC0019172). Funding for fieldwork housing and logistical support was provided by the DOE Atmospheric Radiation Measurement (DOE ARM field campaign 2013-6660). UIC-Science and the DOE ARM Climate Research Facility are thanked for fieldwork assistance in Utqiaġvik, AK. CCSEM-EDX analyses were performed at the Environmental Molecular Sciences Laboratory, a national scientific user facility located at the Pacific Northwest National Laboratory (PNNL) and sponsored by the Office of Biological and Environmental Research of the US DOE. PNNL is operated for the DOE by the Battelle Memorial Institute under contract no. DE-AC06-76RL0 1830. Travel funds to PNNL were provided by the University of Michigan (UM) Rackham Graduate School. ARM data (https://dx.doi.org/10.5439/1786358) were obtained with support from the US DOE Office of Science, Office of Biological and Environmental Research, Climate and Environmental Sciences Division. We acknowledge use of the NOAA Air Resources Laboratory for the provision of the HYSPLIT transport and dispersion model and READY website (https://www.ready.noaa.gov/index.php) used in this publication. STXM-NEXAFS analysis was performed at the Canadian Light Source. Atomic force microscopy was conducted at the Scanning Probe Microscopy facility in the UM Department of Chemistry; Prof. Mark Banaszak-Holl and Dr. Rachel Merzel are thanked for assistance with the initial AFM. Yao Xiao is thanked for assistance with SPIP analysis. This publication is partially funded by the Joint Institute for the Study of the Atmosphere and Ocean under NOAA Cooperative Agreement NA15OAR4320063, Contribution No. 2020-1081. This is Pacific Marine Environmental Laboratory contribution number 5127.

1. D. K. Farmer, C. D. Cappa, S. M. Kreidenweis, Atmospheric processes and their controlling influence on cloud condensation nuclei activity. *Chem. Rev.* **115**, 4199–4217 (2015).
2. N. Riemer, A. P. Ault, M. West, R. L. Craig, J. H. Curtis, Aerosol mixing state: Measurements, modeling, and impacts. *Rev. Geophys.* **57**, 187–249 (2019).
3. Y. Zhang *et al.*, Effect of the aerosol-phase state on secondary organic aerosol formation from the reactive uptake of isoprene-derived epoxydiols (IEPOX). *Environ. Sci. Technol. Lett.* **5**, 167–174 (2018).
4. T. Berkemeier, M. Shiraiwa, U. Pöschl, T. Koop, Competition between water uptake and ice nucleation by glassy organic aerosol particles. *Atmos. Chem. Phys.* **14**, 12513–12531 (2014).
5. R. C. Moffet, K. A. Prather, In-situ measurements of the mixing state and optical properties of soot with implications for radiative forcing estimates. *Proc. Natl. Acad. Sci. U.S.A.* **106**, 11872–11877 (2009).
6. T. Koop, J. Bookhold, M. Shiraiwa, U. Pöschl, Glass transition and phase state of organic compounds: Dependency on molecular properties and implications for secondary organic aerosols in the atmosphere. *Phys. Chem. Chem. Phys.* **13**, 19238–19255 (2011).
7. L. Renbaum-Wolff *et al.*, Viscosity of α-pinene secondary organic material and implications for particle growth and reactivity. *Proc. Natl. Acad. Sci. U.S.A.* **110**, 8014–8019 (2013).
8. M. Shiraiwa *et al.*, Global distribution of particle phase state in atmospheric secondary organic aerosols. *Nat. Commun.* **8**, 15002 (2017).

9. S. Zhou *et al.*, Multiphase reactivity of polycyclic aromatic hydrocarbons is driven by phase separation and diffusion limitations. *Proc. Natl. Acad. Sci. U.S.A.* **116**, 11658–11663 (2019).
10. B. Wang *et al.*, Airborne soil organic particles generated by precipitation. *Nat. Geosci.* **9**, 433–437 (2016).
11. J. P. Reid *et al.*, The viscosity of atmospherically relevant organic particles. *Nat. Commun.* **9**, 956 (2018).
12. R. A. Zaveri *et al.*, Particle-phase diffusion modulates partitioning of semivolatile organic compounds to aged secondary organic aerosol. *Environ. Sci. Technol.* **54**, 2595–2605 (2020).
13. D. J. Cziczo, J. P. D. Abbatt, Deliquescence, efflorescence, and supercooling of ammonium sulfate aerosols at low temperature: Implications for cirrus cloud formation and aerosol phase in the atmosphere. *J. Geophys. Res. D Atmospheres* **104** (D11), 13781–13790 (1999).
14. T. B. Onasch *et al.*, Infrared spectroscopic study of the deliquescence and efflorescence of ammonium sulfate aerosol as a function of temperature. *J. Geophys. Res. D Atmospheres* **104** (D17), 21317–21326 (1999).
15. J. Xu, D. Imre, R. McGraw, I. Tang, Ammonium sulfate: Equilibrium and metastability phase diagrams from 40 to -50°C. *J. Phys. Chem. B* **102**, 7462–7469 (1998).
16. P. Wyszyński, R. Przybylak, Variability of humidity conditions in the Arctic during the first International Polar Year, 1882–83. *Polar Res.* **33**, 23896 (2014).
17. A. L. Bondy *et al.*, Atomic force microscopy-infrared spectroscopy of individual atmospheric aerosol particles: Subdiffraction limit vibrational spectroscopy and morphological analysis. *Anal. Chem.* **89**, 8594–8598 (2017).
18. N. E. Olson *et al.*, Reactive uptake of isoprene epoxydiols increases the viscosity of the core of phase-separated aerosol particles. *ACS Earth Space Chem.* **3**, 1402–1414 (2019).
19. I. Schmitz, M. Schreiner, G. Friedbacher, M. Grasserbauer, Phase imaging as an extension to tapping mode AFM for the identification of material properties on humidity-sensitive surfaces. *Appl. Surf. Sci.* **115**, 190–198 (1997).
20. S. Yamashita *et al.*, Atomic number dependence of Z contrast in scanning transmission electron microscopy. *Sci. Rep.* **8**, 12325 (2018).
21. H. D. Lee, K. K. Ray, A. V. Tivanski, Solid, semisolid, and liquid phase states of individual submicrometer particles directly probed using atomic force microscopy. *Anal. Chem.* **89**, 12720–12726 (2017).
22. D. P. Veghte, D. R. Bittner, M. A. Freedman, Cryo-transmission electron microscopy imaging of the morphology of submicrometer aerosol containing organic acids and ammonium sulfate. *Anal. Chem.* **86**, 2436–2442 (2014).
23. R. J. Hopkins *et al.*, Chemical speciation of sulfur in marine cloud droplets and particles: Analysis of individual particles from the marine boundary layer over the California current. *J. Geophys. Res. D Atmospheres* **113**, 1–15 (2008).
24. A. Dazzi *et al.*, AFM-IR: Combining atomic force microscopy and infrared spectroscopy for nanoscale chemical characterization. *Appl. Spectrosc.* **66**, 1365–1384 (2012).
25. R. Dong, L. E. Yu, Investigation of surface changes of nanoparticles using TM-AFM phase imaging. *Environ. Sci. Technol.* **37**, 2813–2819 (2003).
26. K. J. Baustian, M. E. Wise, M. A. Tolbert, Depositional ice nucleation on solid ammonium sulfate and glutaric acid particles. *Atmos. Chem. Phys.* **10**, 2307–2317 (2010).
27. C. S. Pearson, K. D. Beyer, Solid/liquid phase diagram of the ammonium sulfate/succinic acid/water system. *J. Phys. Chem. A* **119**, 4317–4328 (2015).
28. M. A. Zawadowicz, S. R. Proud, S. S. Seppalainen, D. J. Cziczo, Hygroscopic and phase separation properties of ammonium sulfate/organics/water ternary solutions. *Atmos. Chem. Phys.* **15**, 8975–8986 (2015).
29. D. Q. Pham *et al.*, Biological impacts on carbon speciation and morphology of sea spray aerosol. *ACS Earth Space Chem.* **1**, 551–561 (2017).
30. L. N. Hawkins, L. M. Russell, Polysaccharides, proteins, and phytoplankton fragments: Four chemically distinct types of marine primary organic aerosol classified by single particle spectromicroscopy. *Adv. Meteorol.* **2010**, 1–14 (2010).
31. H. Yu *et al.*, Organic coating on sulfate and soot particles during late summer in the Svalbard Archipelago. *Atmos. Chem. Phys.* **19**, 10433–10446 (2019).
32. S. D. Brooks, M. E. Wise, M. Cushing, M. A. Tolbert, Deliquescence behavior of organic/ammonium sulfate aerosol. *Geophys. Res. Lett.* **29**, 23–1–23-4 (2002).
33. M. A. Freedman, Liquid-liquid phase separation in supermicrometer and submicrometer aerosol particles. *Acc. Chem. Res.* **53**, 1102–1110 (2020).
34. R. D. Davis, S. Lance, J. A. Gordon, S. B. Ushijima, M. A. Tolbert, Contact efflorescence as a pathway for crystallization of atmospherically relevant particles. *Proc. Natl. Acad. Sci. U.S.A.* **112**, 15815–15820 (2015).
35. R. Zhang, Atmospheric science. Getting to the critical nucleus of aerosol formation. *Science* **328**, 1366–1367 (2010).
36. S. B. Ushijima, E. Huynh, R. D. Davis, M. A. Tolbert, Seeded crystal growth of internally mixed organic-inorganic aerosols: Impact of organic phase state. *J. Phys. Chem. A* **125**, 8668–8679 (2021).
37. M. J. Gunsch *et al.*, Contributions of transported Prudhoe Bay oil field emissions to the aerosol population in Utqiaġvik, Alaska. *Atmos. Chem. Phys.* **17**, 10879–10892 (2017).
38. B. Croft *et al.*, Processes controlling the annual cycle of Arctic aerosol number and size distributions. *Atmos. Chem. Phys.* **16**, 3665–3682 (2016).
39. L. J. Beck *et al.*, Differing mechanisms of new particle formation at two arctic sites. *Geophys. Res. Lett.* **48**, e2020GL091334 (2021).
40. M. Giamarelou *et al.*, Indirect evidence of the composition of nucleation mode atmospheric particles in the high arctic. *J. Geophys. Res.* **121**, 965–975 (2016).
41. E. L. Mungall *et al.*, Microlayer source of oxygenated volatile organic compounds in the summertime marine Arctic boundary layer. *Proc. Natl. Acad. Sci. U.S.A.* **114**, 6203–6208 (2017).
42. B. Croft *et al.*, Contribution of Arctic seabird-colony ammonia to atmospheric particles and cloud-albedo radiative effect. *Nat. Commun.* **7**, 13444 (2016).
43. R. Ghahremaninezhad *et al.*, Dimethyl sulfide and its role in aerosol formation and growth in the Arctic summer – A modelling study. *Atmos. Chem. Phys.* **19**, 14455–14476 (2019).
44. S. Tremblay *et al.*, Characterization of aerosol growth events over Ellesmere Island during the summers of 2015 and 2016. *Atmos. Chem. Phys.* **19**, 5589–5604 (2019).
45. C. R. Ruehl, K. R. Wilson, Surface organic monolayers control the hygroscopic growth of submicrometer particles at high relative humidity. *J. Phys. Chem. A* **118**, 3952–3966 (2014).
46. G. P. Schill, M. A. Tolbert, Heterogeneous ice nucleation on phase-separated organic-sulfate particles: Effect of liquid vs. glassy coatings. *Atmos. Chem. Phys.* **13**, 4681–4695 (2013).
47. A. Tandon, N. E. Rothfuss, M. D. Petters, The effect of hydrophobic glassy organic material on the cloud condensation nuclei activity of particles with different morphologies. *Atmos. Chem. Phys.* **19**, 3325–3339 (2019).
48. J. P. D. Abbatt *et al.*, Solid ammonium sulfate aerosols as ice nuclei: A pathway for cirrus cloud formation. *Science* **313**, 1770–1773 (2006).
49. H. Morrison *et al.*, Resilience of persistent Arctic mixed-phase clouds. *Nat. Geosci.* **5**, 11–17 (2012).
50. M. C. Serreze, R. G. Barry, Processes and impacts of Arctic amplification: A research synthesis. *Global Planet. Change* **77**, 85–96 (2011).
51. P. K. Quinn, D. J. Coffman, J. E. Johnson, L. M. Upchurch, T. S. Bates, Small fraction of marine cloud condensation nuclei made up of sea spray aerosol. *Nat. Geosci.* **10**, 674 (2017).
52. M. Årthun, I. H. Onarheim, J. Dörr, T. Eldevik, The seasonal and regional transition to an ice-free arctic. *Geophys. Res. Lett.* **48**, e2020GL090825 (2021).
53. D. Kwon *et al.*, Optical property measurements and single particle analysis of secondary organic aerosol produced from the aqueous-phase reaction of ammonium sulfate with methylglyoxal. *ACS Earth Space Chem.* **2**, 356–365 (2018).
54. R. C. Moffet, T. Henn, A. Laskin, M. K. Gilles, Automated chemical analysis of internally mixed aerosol particles using X-ray spectromicroscopy at the carbon K-edge. *Anal. Chem.* **82**, 7906–7914 (2010).